NANO · MICRO small
www.small-journal.com

In Situ CVD Derived Co–N–C Composite as Highly Efficient Cathode for Flexible Li–O_2 Batteries

Zhen-Dong Yang, Xiao-Yang Yang, Tong Liu, Zhi-Wen Chang, Yan-Bin Yin, Xin-Bo Zhang, Jun-Min Yan, and Qing Jiang*

To promote the development of high energy Li–O_2 batteries, it is important to design and construct a suitable and effective oxygen-breathing cathode. Herein, activated cobalt-nitrogen-doped carbon nanotube/carbon nanofiber composites (Co-N-CNT/CNF) as the effective cathodes for Li–O_2 batteries are prepared by in situ chemical vapor deposition (CVD). The unique architecture of these electrodes facilitates the rapid oxygen diffusion and electrolyte penetration. Meanwhile, the nitrogen-doped carbon nanotube/carbon nanofiber (N-CNT/CNF) and Co/CoN_x serve as reaction sites to promote the formation/decomposition of discharge product. Li–O_2 batteries with Co-N-CNT/CNF cathodes exhibit superior electrochemical performance in terms of a positive discharge plateau (2.81 V) and a low charge overpotential (0.61 V). Besides, Li–O_2 batteries also present a high discharge capacity (11512.4 mAh g^{-1} at 100 mA g^{-1}), and a long cycle life (130 cycles). Meanwhile, the Co-N-CNT/CNF cathode also has an excellent flexibility, thus the assembled flexible battery with Co-N-CNT/CNF can work normally and hold a wonderful capacity rate under various bending conditions.

Rechargeable aprotic lithium–oxygen (Li–O_2) battery has received enormous attention as one of promising next-generation batteries because of its high theoretical energy density (3600 Wh kg^{-1}), which could power electric vehicles (EVs) with a driving range comparable to gasoline powered automobile.[1–3] Different from the state-of-the-art Li-ion battery, the Li–O_2 battery is based on the reversible formation/decomposition of Li_2O_2 ($2Li^+ + O_2 + 2e^- \leftrightarrow Li_2O_2$, $\Delta E = 2.96$ V), including oxygen reduction reaction (ORR) and oxygen evolution reaction (OER) in the cycling process. However, the kinetics of ORR and OER reactions is sluggish, which results in large discharge/charge overpotentials. Simultaneously, the random deposition of discharge product would block the permeation path for oxygen and electrolyte within the cathode, resulting in serious decay in the capacity and cycling stability of the battery. All these above challenges limit the practical application of Li–O_2 batteries.[4–8] Therefore, preparing an effective cathode with high bifunctional catalysts would be conductive to improving the performances of Li–O_2 battery. Additionally, the involvement of electrochemically inactive polymer binders in the traditional cathode fabrication, such as polytetrafluoroethylene and polyvinylidene fluoride, may concurrently occupy the porous channels, thus blocking the diffusion of oxygen and electrolyte, limiting the specific capacities of Li–O_2 batteries.[9–11] And the organic binders would suffer from nucleophilic attack of high-sensitive intermediated radicals, decomposing to generate LiF, LiOH, and Li_2CO_3, thus deteriorating the surface of the electrode.[12–14]

To mitigate these above mentioned problems, one promising approach is to build a binder-free electrode with high ORR/OER activities and a self-standing structure. Carbon nanofiber (CNF) or carbon nanotube (CNT), both as 1D materials, have been proposed as desirable choices as electrodes for batteries due to their advantageous properties, such as remarkable electrical conductivity, large surface area, and high mechanical strength.[15,16] In addition, by simply using appropriate reagents containing heteroatoms, such as N, S, and P, as the precursor solution in electrode preparation process, more catalytic activity sites could be obtained in CNF or CNT. As a result, heteroatoms-doped CNF and CNT are promising electrodes with excellent ORR activity in Li–O_2 batteries. However, their poor OER activity would lead to a high charge voltage being over 4.5 V, resulting in a poor energy efficiency.[17–19] To address the limitation on OER catalysis, several carbon-based noble metals (Ru, Pt, and RuO_2) have been successfully synthesized and they possess high electrocatalytic activity in Li–O_2 batteries, but their high cost and scarcity largely hinder the large-scale practical allocation of them.[20–22] Therefore, extensive efforts have been made to develop earth-abundant and low-cost transition metals, such as transition metal nanoparticles, transition metal oxides/sulfides/nitrides as well as transition metal and nitrogen cofunctionalized carbon materials.[9,23–26] Among all candidates, cobalt-based N-doped carbon compounds gain excellent performances and have received considerable attention as

Z.-D. Yang, X.-Y. Yang, Dr. Y.-B. Yin, Prof. J.-M. Yan, Prof. Q. Jiang
Key Laboratory of Automobile Materials (Jilin University) of Education
School of Materials Science and Engineering
Jilin University
Changchun 130022, China
E-mail: junminyan@jlu.edu.cn
Z.-D. Yang, X.-Y. Yang, T. Liu, Z.-W. Chang, Dr. Y.-B. Yin, Prof. X.-B. Zhang
State Key Laboratory of Rare Earth Resource Utilization
Changchun Institute of Applied Chemistry
Chinese Academy of Sciences
Changchun 130022, P. R. China
Z.-W. Chang
University of Chinese Academy of Sciences
Beijing 100049, P. R. China

DOI: 10.1002/smll.201800590

catalysts in metal–air batteries, owing to the superior OER activity of Co/CoN_x and the promising ORR activity of N-doped carbon.[17,27–30]

With the above understanding in mind, we design a novel in situ CVD to grow carbon nanotube on the surface of cobalt-nitrogen-doped carbon nanofiber by calcining melamine to produce graphitic carbon nitride that serves as carbon and nitrogen source under the effect of Co nanoparticles, yielding the activated cobalt-nitrogen-doped carbon nanotube/carbon nanofiber composite (Co-N-CNT/CNF). Conventionally, CNT are prepared via using liquid chemical vapor deposition method, which requires costly equipment and a high temperature as well as a special or toxic atmosphere. While our method is inexpensive and facile via an in situ CVD method without using any special or toxic atmosphere. Unexpectedly, the Co-N-CNT/CNF cathodes endow Li–O_2 batteries with superior electrochemical performances, including low overpotentials, a good rate capability, and an excellent cycle stability, which might be due to the synergistic effect of the structure of the CNT/CNF and the superior catalytic activity of Co/CoN_x:CNTs on the surface of CNFs could provide strong and stable interconnectivity between the active actives and the electrode, thus promote the rapid transfer of electrons and enhance the catalytic activity of electrode. Moreover, the hierarchical and porous structure of CNT/CNF is a boon to enable rapid oxygen and electrolyte diffusion, another key factor in improving the practical catalytic activity. Besides, Co/CoN_x would serve as the growth sites of Li_2O_2 and regulate the formation of isolated nanosheets of Li_2O_2, which could provide sufficient Li_2O_2–electrolyte interfaces, thus enhance the rechargeability of the Li–O_2 cell. Surprisingly, Co-N-CNT/CNF cathode performances a superior flexibility, and the as-prepared flexible Li–O_2 battery in different shapes could power a commercial red light emitting diode (LED) and hold a good rate capacity.

Scheme 1 illustrates the synthesis strategy of Co-N-CNT/CNF. First, the self-standing Co-rich polymer fibers film was obtained by the electrospinning technology. Then the polymer fibers film was stabilized in air at 280 °C with the dehydrogenation and cyclization process. During sintering process, PAN would be transferred to a ladder structure consisting of a series of connected C–N aromatic rings. This structure could be maintained at an even high temperature.[31,32] After that, the stabilized film was carbonized at 750 °C in the presence of melamine under an inert atmosphere. During carbonization process, CA would completely decompose, leaving channels to expose the transition metal compositions. Then under the effect of Co nanoparticles formed by the decomposition of $Co(Acac)_2$, CNTs were in situ grown on the surface of CNFs with the pyrolytic product of melamine severing as both the nitrogen and carbon sources.[33–36] Finally, Co-N-CNT/CNF was cut into slices with a diameter of 12 mm to be directly used as cathodes for Li–O_2 batteries.

As shown in **Figure 1**a, the composite Co-N-CNT/CNF is analyzed by X-ray diffraction (XRD). All diffraction peaks match well with the standard powder diffraction of Co crystalline structure (JCPDS: 15-0806).[37] Then, the morphology and porous structure of Co-N-CNT/CNF are investigated using field emission scanning electron microscopy (SEM) and transmission electron microscopy (TEM). When compared with N–CNF (Figure S1, Supporting Information) and Co-N-CNF (Figure S2, Supporting Information), CNTs in situ grow on CNFs uniformly without the help of any additional binders. As a benefit, the CNT-modified would increase the active surface area and further enhance the catalytic performance of the material (Figure 1b,c). And even bent to 180°, the Co-N-CNT/CNF could still keep its mechanical structure (Figure S3, Supporting Information), demonstrating its potential application as a flexible electrode for Li–O_2 battery. Compared with other liquid CVD method, this CNT-modified method is a low-cost and facile strategy.[34,36,38,39] The low magnification TEM image (Figure 1d) of the Co-N-CNT/CNF further reveals that CNTs twines on CNF substrate, and many Co nanoparticles randomly disperse on CNFs and CNTs. Then the high-magnification TEM illustrates that CNT has a multiwall structure (yellow oval area in Figure 1e) with a diameter of about 13.588 nm. Simultaneously, the *d*-spacing of Co nanoparticles is found to

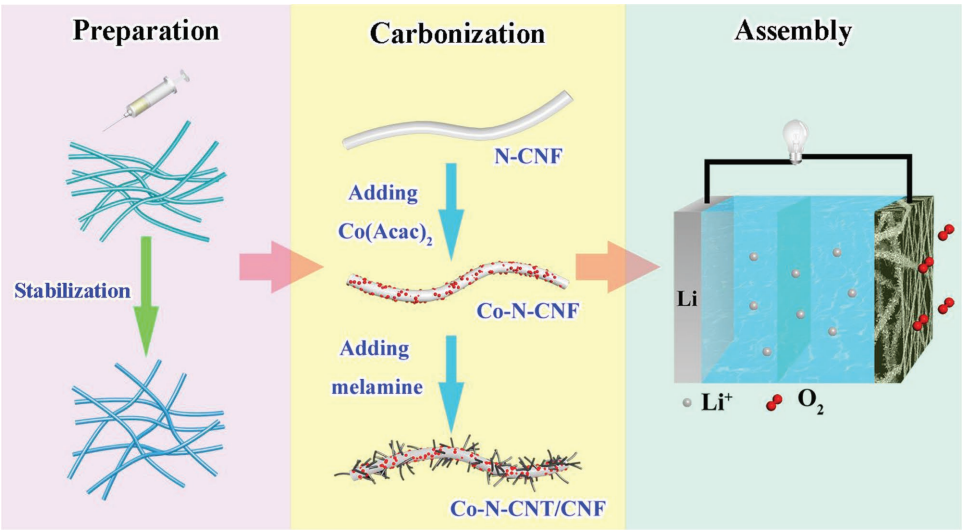

Scheme 1. Schematic illustration of the preparation process for the binder-free and self-standing Co-N-CNT/CNF.

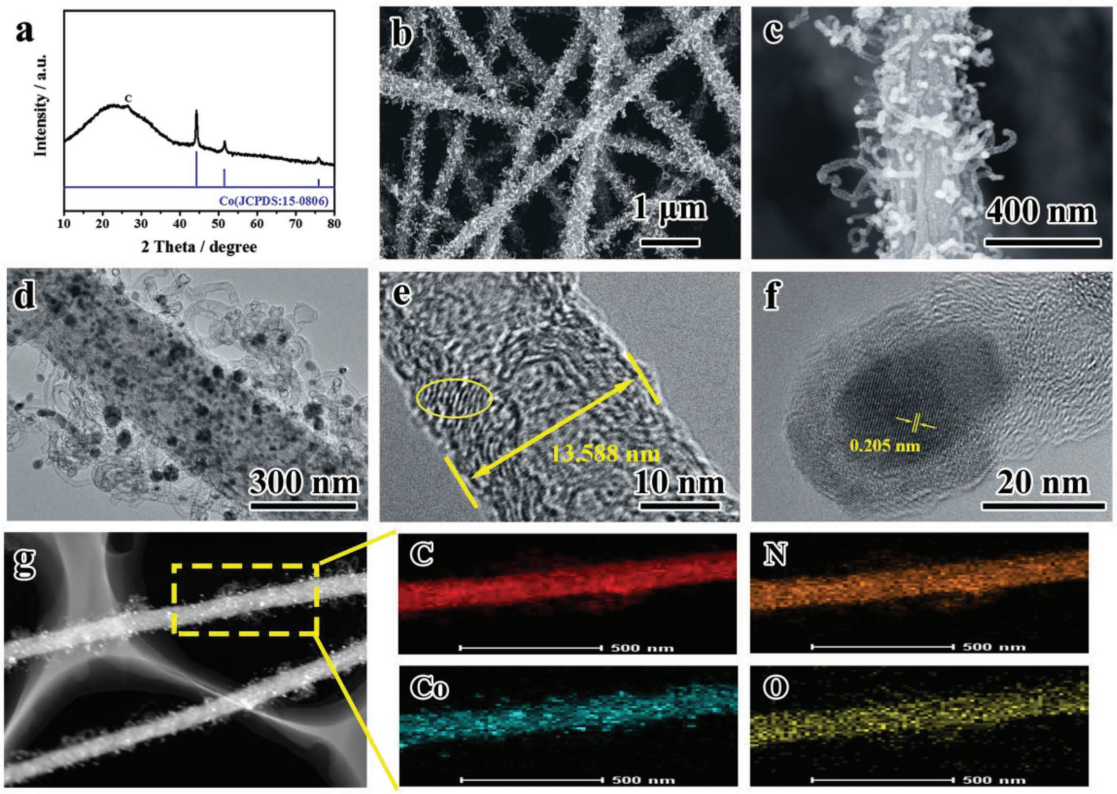

Figure 1. a) XRD pattern of Co-N-CNT/CNF. b) Low and c) high magnification SEM images of Co-N-CNT/CNF. d) Low magnification TEM image of Co-N-CNT/CNF. e) High magnification TEM image of CNT on the Co-N-CNT/CNF. f) High magnification TEM image of Co nanoparticle on Co-CNT/CNF. g) Elemental mapping of Co-N-CNT/CNF.

be 0.205 nm, corresponding to the (111) plane of Co (JCPDS: 15-0806). And the corresponding EDX elemental mapping (Figure 1g) demonstrates that C, N, Co, and O atoms are homogeneously distributed throughout the electrode.

To further investigate the surface area and porosity of Co-N-CNT/CNF cathode, the N_2 adsorption–desorption plots of Co-N-CNT/CNF are measured. As shown in **Figure 2**a, typical type-IV isotherms indicate that the Co-N-CNT/CNF possess a mesoporous nature. The Brunauer–Emmett–Teller surface area of Co-CNT/CNF is 116.507 m^2 g^{-1}, and the pore distribution has a major peak at 4 nm calculated from the Barrett–Joyner–Halenda method.[40,41] Afterward, Raman spectra of Co-N-CNT/CNF cathode and its contrasts are performed to analyze the effect of the Co-N-doped and CNT-modified on the as-prepared fibers. As shown in Figure 2b, there are two remarkable peaks at around 1350 and 1590 cm^{-1} on the Raman spectra. They are D band (the structural defects and partially disordered structures) and G band (the E_{2g} vibration mode of sp^2 carbon domains) of carbon, respectively. Note that the ratio of the integrated intensities of D band to G band in the Co-N-CNT/CNF cathode (I_D/I_G = 1.00) is higher than these of Co–N–CNF cathode and N-CNF cathode, meaning

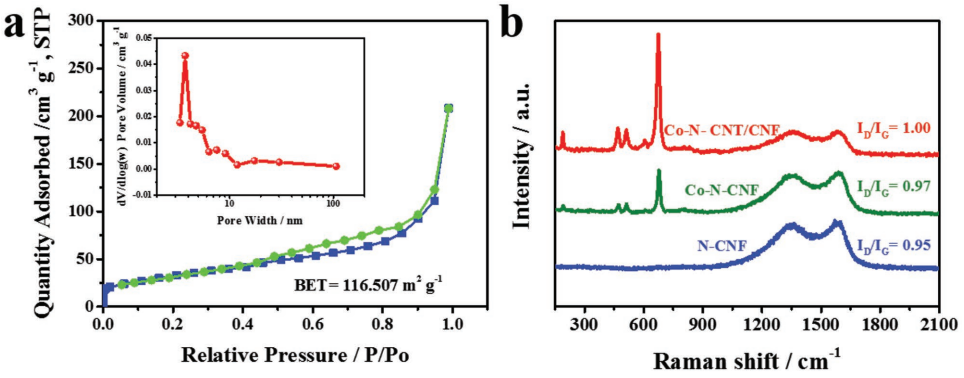

Figure 2. a) N_2 adsorption–desorption isotherms and pore-size distribution (inset) of the Co-N-CNT/CNF. b) Raman spectra of three different cathodes.

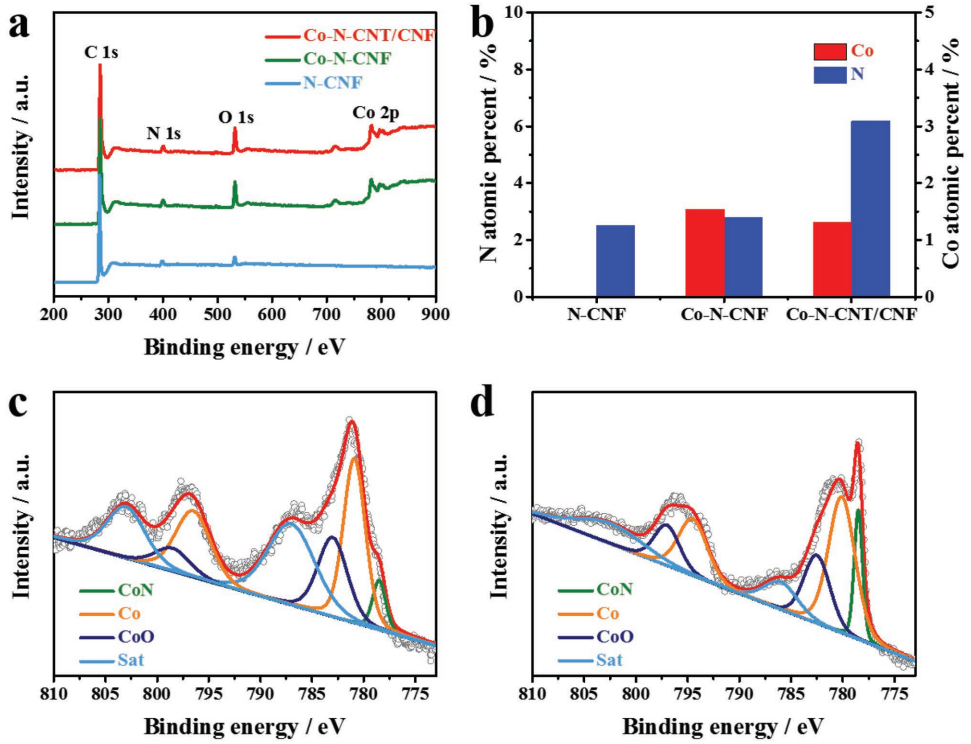

Figure 3. a) XPS survey spectra of N-CNF, Co-N-CNF, and Co-N-CNT/CNF. b) Atomic percent of N and Co in N-CNF, Co-N-CNF, and Co-N-CNT/CNF. High-resolution XPS spectra of Co 2p in c) Co–CNF and d) Co-CNT/CNF.

that there are more active sites in Co-N-CNT/CNF due to the Co-N-doped and CNT-modified.[36,42,43] Notably, new peaks at 200–700 cm^{-1} appearing in the spectra of Co-N-CNT/CNF and Co-N-CNF could be attributed to the modes of Co or CoO, respectively.[23,42,44]

X-ray photoelectron spectroscopy (XPS) characterizations are further performed to compare the changes of elemental composition in Co-N-CNT/CNF and its contrasts. As is shown in **Figure 3**a, the XPS spectrum of N-CNF shows only the presence of carbon, nitrogen and oxygen atoms. After the Co-doped and CNT-modified, the intensity of cobalt and nitrogen increase a lot in the XPS survey spectra of Co-N-CNF and Co-N-CNT/CNF. Figure 3b and Table S1 (Supporting Information) reveal in detail that the changes in the content of each element in different samples. We guess that the decrease of oxygen content is due to the reduction of the oxygen-containing functional groups under the effect of cobalt nanoparticles. The pyrolysis of the melamine further increases the content of nitrogen in Co-N-CNT/CNF cathode. The high Co/N content and principally high density of active sites of Co-N-CNT/CNF cathode are believed to be highly favorable for enhancing the performances of Li–O_2 batteries. To further study the chemical states of cobalt in Co-N-CNF and Co-N-CNT/CNF, the spectrum of Co 2p in these samples are analyzed in detail (Figure 3c,d), the peak centered at 781.2 eV is ascribed to Co $2p_{3/2}$ with a shakeup satellite at 786.4 eV and the peak centered at 796.8 eV is assigned to CoO $2p_{1/2}$ with a shakeup satellite at 802.8 eV. These peaks obviously suggest the presence of metallic Co and CoO through Gaussian fitting. CoO mainly stems from the surface oxidation of Co nanoparticles during the XPS test procedure. Besides, the peaks at 779.1 eV is ascribed to Co-N bond, meaning that the CoN_x compound exits in Co–N–CNF and especially in Co-N-CNT/CNF.[23,29,45] In a word, Co-doping promotes the formation of Co/CoN_x composite in both Co-N-CNF and Co-N-CNT/CNF. Similarly, the bonding configurations of nitrogen atoms in these samples are also characterized by high-resolution N1s spectra. The N1s spectra of these samples can be fitted into four peaks at 398.2, 399.5, 401.1, and 402.6 eV (**Figure 4**a–c), indicating the discovery of four different bonding states of N, i.e., pyridinic-N (N1), pyrrolic-N (N2), graphitic-N (N3), and oxydic-N (N4), respectively.[36,46,47] The 398.2 eV peak may also include contributions from CoN_x because the difference between the binding energies of CoN_x and pyridinic-N is small. The relative N content of these samples is summarized in Figure 4d and Table S2 (Supporting Information). It is worthy to note that the pyrolysis process of melamine increases the N content a lot in Co-N-CNT/CNF. And the content of pyridinic-N and graphitic-N increases a lot under the effect of Co nanoparticles. More importantly, pyridinic-N and graphitic-N have a great ORR activity in Li–O_2 battery.[40,48]

As a proof-of-concept, the electrochemical properties of Co-N-CNT/CNF are then analyzed in Li–O_2 batteries. Meanwhile, Co-N-CNT and N-CNF are also employed as electrodes in Li–O_2 batteries for comparison. All electrochemical measurement results are normalized based on the total weight of the cathode. **Figure 5**a shows the first discharge-charge voltage of Li–O_2 batteries with Co-N-CNT/CNF, Co-N-CNF, N-CNF at a current density of 200 mA g^{-1} with a limited capacity of 1000 mAh g^{-1}. The discharge-charge gap of Co-CNT/CNF is only 0.76 V, lower than that of Co-N-CNF (1.02 V) and N-CNF (1.63 V). In detail,

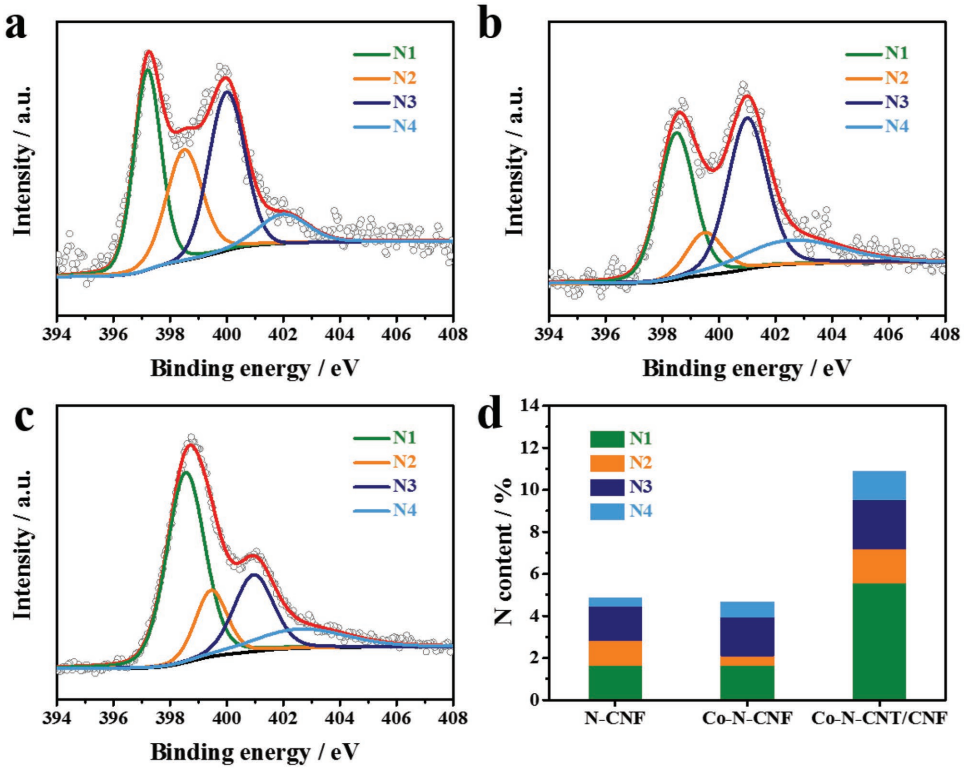

Figure 4. High-resolution N1s spectra of a) N-CNF, b) Co-N-CNF, and c) Co-N-CNT/CNF. d) The proportion of nitrogen atoms in N-CNF, Co-N-CNF, and Co-N-CNT/CNF.

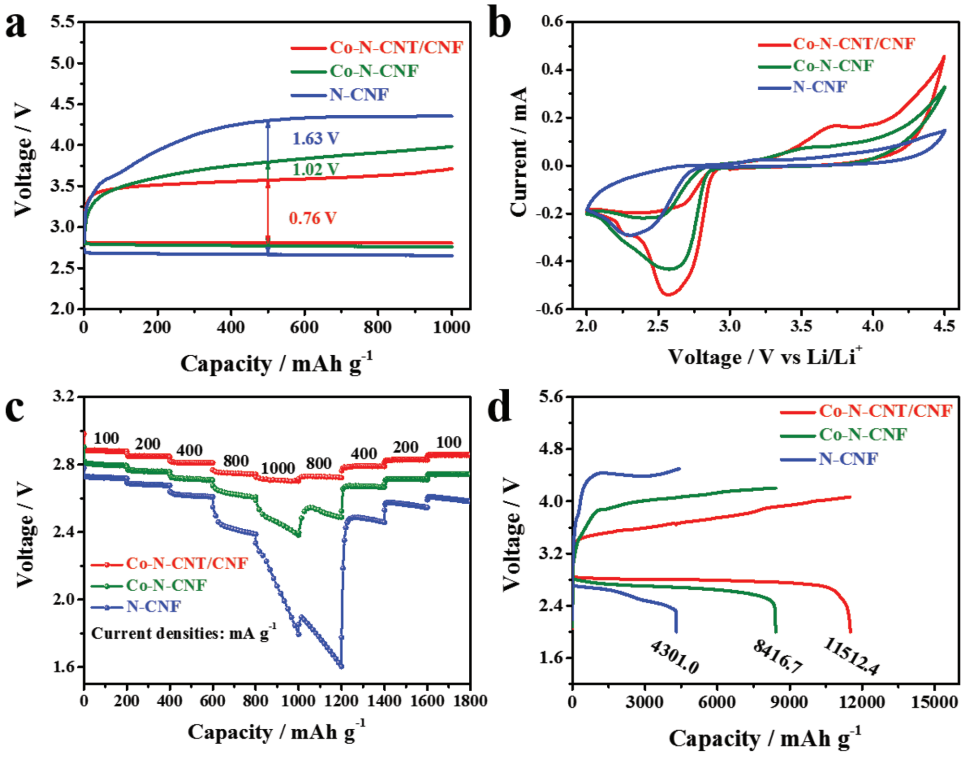

Figure 5. a) First discharge–charge curves of the Li–O_2 battery with three cathodes at a current density of 200 mA g^{-1}. b) CV profiles of the Li–O_2 battery with three different cathodes at voltage sweep rate of 0.5 mV s^{-1}. c) The rate capability of the Li–O_2 batteries with three cathodes at different current densities. d) Full range discharge test of the Li–O_2 batteries with three different cathodes at a current density of 100 mA g^{-1}.

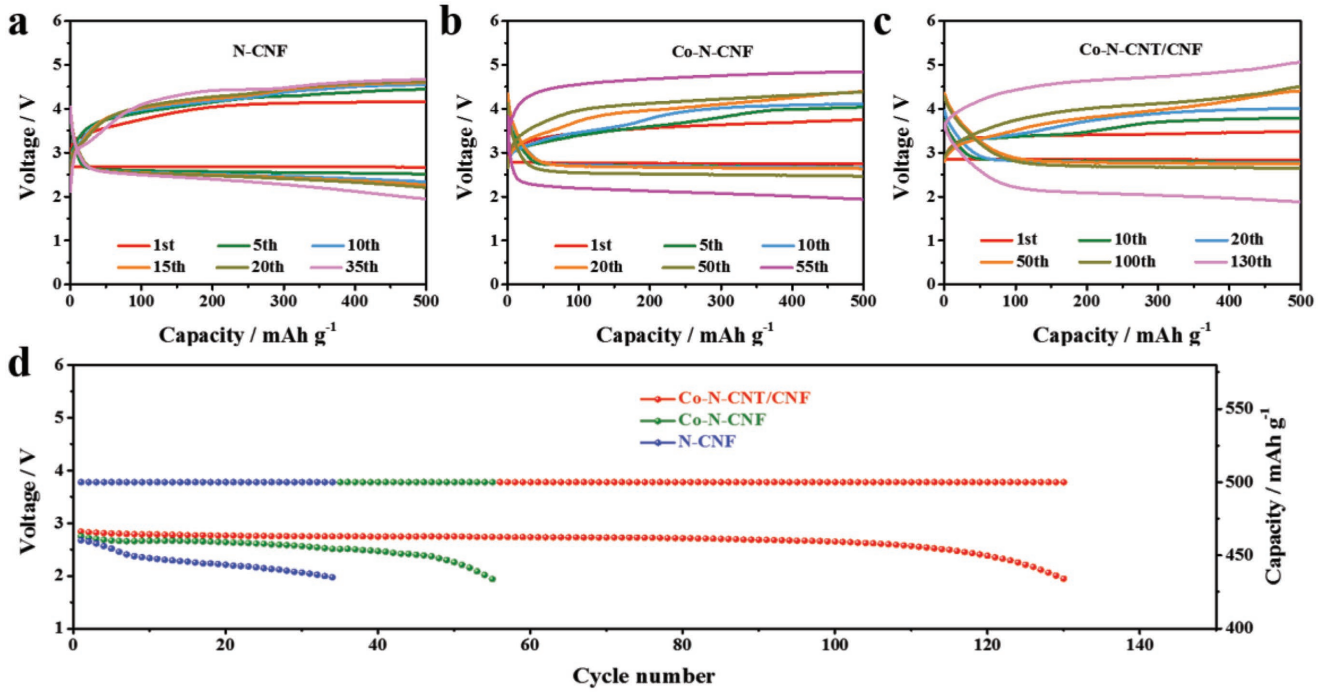

Figure 6. The discharge–charge curves of a) N-CNF, b) Co–N–CNF, and c) Co-N-CNT/CNF cathode for Li–O_2 battery at a current density of 200 mA g^{-1} with a specific capacity of 500 mAh g^{-1}. d) The terminal discharge voltage of Li–O_2 batteries with three different cathodes.

Co-N-CNT/CNF displays a higher discharge voltage plateau (2.81 V) than that of N-CNF (2.67 V) and slightly higher than that of Co-N-CNF (2.77 V). Surprisingly, the charge overpotential of Co-N-CNT/CNF is only 0.61 V, which is lower than that of Co–N–CNF (0.83 V) and N–CNF (1.34 V). To obtain further insights into the electrochemical activity of Co-N-CNT/CNF cathode and its contrasts, cyclic voltammetry (CV) is performed for ORR and OER at a scan rate of 0.5 mV s^{-1}. The cycle curve reveals that the Co-N-CNT/CNF cathode exhibits a higher ORR onset potential, a lower OER onset potential, and a higher ORR/OER peak current compared with that of Co-N-CNF cathode and N-CNF cathode (Figure 5b).[44,49]

Furthermore, Li–O_2 batteries with Co-N-CNT/CNF cathodes hold a higher discharge potential than those with Co-N-CNT/CNF and N-CNF under different current densities (Figure 5c), confirming the relatively high rate performance of the Li–O_2 batteries with Co-N-CNT/CNF cathodes. Additionally, Co-N-CNT/CNF cathode also delivers a much higher discharge specific capacity (11512.4 mAh g^{-1}) than that of Co-N-CNF (8416.7 mAh g^{-1}) and N-CNF (4301.0 mAh g^{-1}) at the current density of 100 mA g^{-1} (Figure 5d). Unexpectedly, at an even higher current density of 1000 mA g^{-1}, Li–O_2 battery with Co-N-CNT/CNF still exhibits a very high capacity of 3332.0 mAh g^{-1} (Figure S4, Supporting Information). Additionally, to exclude the electrochemical contribution from the Li^+ intercalation into carbon-based carbon, the discharge capacities with the three cathodes in Li–O_2 batteries are also examined under Ar atmosphere (Figure S5, Supporting Information). Obviously, the capacity is negligible within the voltage range, which suggests that ORR is primarily responsible for discharge capacities of the Li–O_2 batteries.[50,51] These results indicate that Co-N-CNT/CNF cathodes possess superior electrochemical performances in Li–O_2 batteries, which might be derived from the synergy of the following advantageous factors: i) the self-standing and binder-free structure of CNF is a boon to enable rapid oxygen and electrolyte diffusion and provides enough void space to house discharged product; ii) in situ growth of active CNTs provide strong and stable interconnectivity between the active materials and the electrode, which enhance the catalytic activity and, more importantly, improve the stability of the cathode; and iii) N-CNT/CNF has great ORR activity and Co/CoN_x composite has enough activity in OER process. Their synergistic effect

Table 1. Comparison of the cycling performances of the Co-N-CNT/CNF cathode with other reported M-CNF electrodes in Li–O_2 batteries.

Cathodes	Cycling performance		Maximum specific capacity	Reference
	Numbers	Measurement condition		
Co-N-CNT/CNF	130 cycles	500 mAh g^{-1} at 200 mA g^{-1}	11512.4 mAh g^{-1} at 100 mA g^{-1}	Our work
Co/CNF-7.4%	50 cycles	500 mAh g^{-1} at 100 mA g^{-1}	4583 mAh g^{-1} at 100 mA g^{-1}	49
Co-PCNF	60 cycles	500 mAh g^{-1} at 100 mA g^{-1}	8800 mAh g^{-1} at 100 mA g^{-1}	57
Fe/Fe_3C-CNF	41 cycles	600 mAh g^{-1} at 300 mA g^{-1}	6250 mAh g^{-1} at 200 mA g^{-1}	58

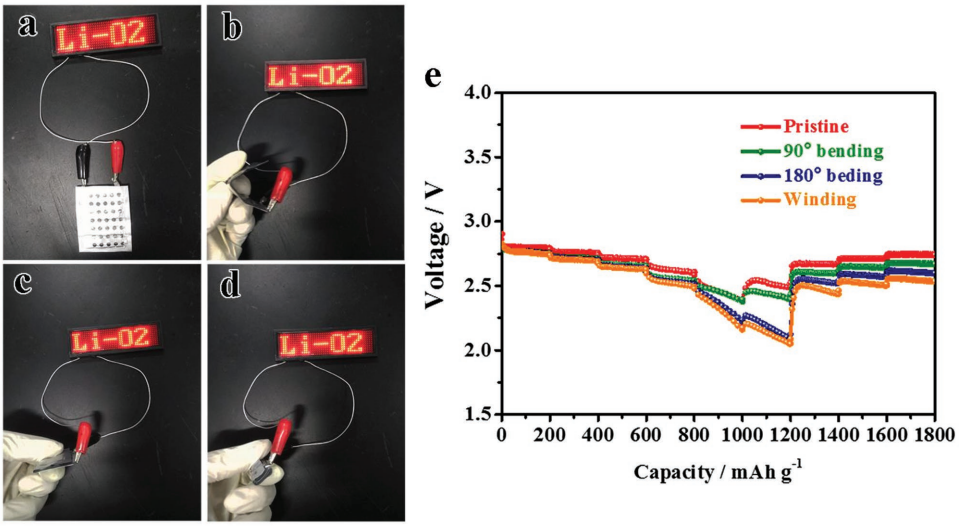

Figure 7. The photographs of the red LED powered by the Li–O_2 batteries when a) pristine, bending, b) 90° bending, c) 180° bending, and d) winding. e) The corresponding rate capability of the Li–O_2 battery with Co-N-CNT/CNF cathode at different shapes.

could realize an efficient formation and decomposition of discharge product Li_2O_2.

Another considerable improvement of Li–O_2 battery with Co-N-CNT/CNF cathode is the cycling stability. **Figure 6** presents the discharge–charge profiles for Li–O_2 batteries with N-CNF, Co-N-CNF, and Co-N-CNT/CNF cathodes at a current density of 200 mA g^{-1} with a fixed capacity of 500 mAh g^{-1}. The Co-N-CNT/CNF cathode can cycle 130 cycles with the discharge terminal being >2.0 V. By contrast, Co-N-CNF and N-CNF cathodes could only cycle 55 and 35 cycles, respectively. This finding confirms that the Co-N-CNT/CNF cathode has a superior cycling stability. To better illustrate the superiority of the Co-N-CNT/CNF cathode, a comparison between the cycling performances of our cathode and those of reported M-CNF (M = Co, Fe) cathode is presented in **Table 1.** Of note, under the similar experiment condition, the cycling performance of the Co-N-CNT/CNF cathode outperforms that of the Co/CNF-7.4%, Co-PCNF, and Fe/Fe_3C-CNF cathodes.[44,52,53] These results further confirm the excellent electrochemistry performance of Co-N-CNT/CNF cathode. To further investigate its application in flexible electronics, the as-prepared flexible Li–O_2 batteries with Co-N-CNT/CNF cathodes are used to power a commercial red light-emitting diode display screen (LED) (**Figure 7**). Excitingly, the assembled flexible battery could still work normally and holds a great rate capacity under various bending conditions, revealing that as-prepared flexible Li–O_2 battery with Co-N-CNT/CNF cathode has an excellent electrochemical stability.

Inspired by the above obtained superior electrochemical performances of Li–O_2 batteries with Co-N-CNT/CNF cathode, we then investigate the discharge products using various methods. After galvanostatic discharge to 2000 mAh g^{-1} at a current density of 200 mA g^{-1}, there are several new peaks in the XRD patterns of these cathodes, which could be reasonably assigned of Li_2O_2 (**Figure 8**a), indicating that discharge product is crystalline Li_2O_2.[25,54] The formation of Li_2O_2 is further evidenced by the galvanostatic intermittent titration technique measurement (Figure S11a, Supporting Information). The equilibrium discharge potential of Li–O_2 battery with Co-N-CNT/CNF cathode is near 2.96 V, which is in accordance with the formation potential of Li_2O_2.[55,56] When the batteries are recharged to 2000 mAh g_{total}^{-1}, the diffraction peaks of Li_2O_2 disappears which suggests that the discharge product

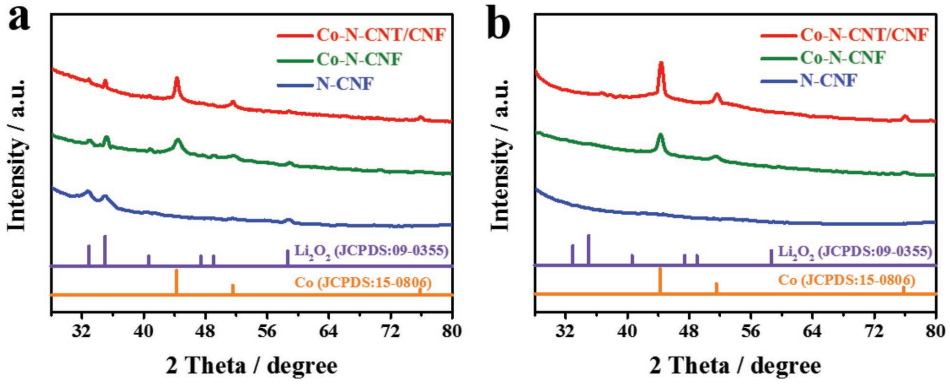

Figure 8. XRD patterns of a) discharged and b) charged N-CNF, Co-N-CNF, and Co-N-CNT/CNF cathodes.

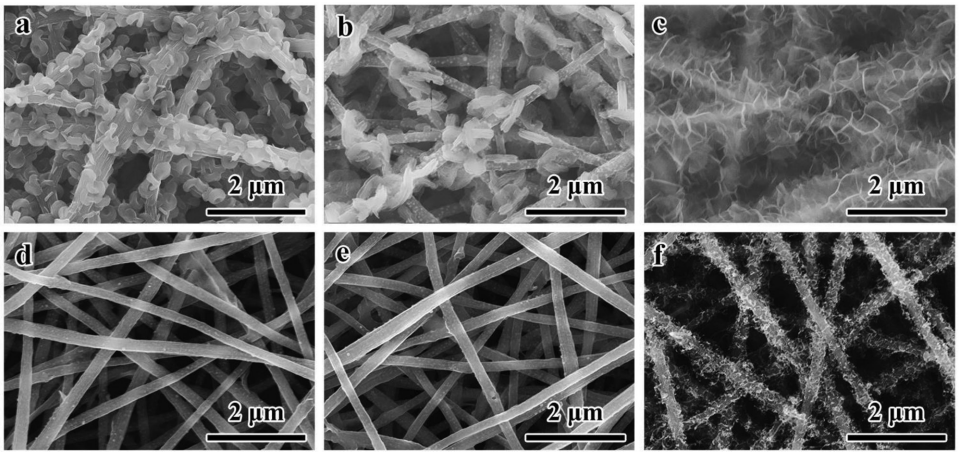

Figure 9. SEM images of discharged a) N-CNF, b) Co-N-CNF, and c) Co-N-CNT/CNF. SEM images of recharged d) N-CNF, e) Co-N-CNF, and f) Co-N-CNT/CNF.

Li_2O_2 is decomposed in the recharging process (Figure 8b), indicating that the rechargeability of these cathodes is very great.

Figure 9 presents SEM images of the morphology of discharge product of different cathodes. The discharge product from the Co-N-CNF cathode is the large toroid-like product, which is much larger than toroid-like product from N-CNF cathode. In sharp contrast, the nanosheet-like discharge product is uniformly and loosely dispersed onto the surface of the Co-N-CNT/CNF cathode, which promote subsequent charge processes and finally enhance the performances of the Li–O_2 battery.[57–59] The SEM images (Figure 7d–f) and TEM images (Figure S12, Supporting Information) after recharged also show the rechargeability of these cathodes. And the electrochemical impedance spectra of Li–O_2 battery with Co-N-CNT/CNF cathode is measured to further investigate the rechargability of Co-N-CNT/CNF cathode. As shown in Figure S11b of the Supporting Information, the impedance of the cell increases significantly, which is due to the very poor electronic conductivity of discharge products generated on the surface of cathode. Pleasurably, after recharging, the impedance of the cell almost gets back to the initial value, indicating that the insulated discharge products can be nearly fully decomposed during charge, which is consistent with the SEM images of Figure 7c,f.

In summary, a binder-free and self-standing Co-N-CNT/CNF composite has been fabricated by a general synthesis strategy combining an electrospinning technique with an in situ CVD approach. The resultant Co-N-CNT/CNF possesses hierarchical and porous structures with CNTs in situ grown on the carbon fiber surface. Due to the high catalytic of N-CNT/CNF and Co/CoN_x composite and the efficient mass-transport of structure, the Co-N-CNT/CNF as a novel electrode demonstrate superior catalytic activity in Li–O_2 batteries. Rechargeable Li–O_2 batteries using Co-N-CNT/CNF as cathodes exhibit excellent battery performances with a low discharge–charge voltage gap (0.67 V), a high discharge capacity (11512.4 mAh g^{-1}), and a long cycle life (130 cycles). And benefitting from the excellent flexibility of the electrodes, the assembled flexible battery can work normally under various bending conditions.

Supporting Information

Supporting Information is available from the Wiley Online Library or from the author.

Acknowledgements

Z.-D.Y., X.-Y.Y., T.L., and Z.-W.C. contributed equally to this work. This work was financially supported by Ministry of Science and Technology of the People's Republic of China (Grant Nos. 2017YFA0206704 and 2016YFB0100103), and The Jiangsu Province Basic Research Program (grant no. BK20140267).

Conflict of Interest

The authors declare no conflict of interest.

Keywords

binder-free, Co–N–C composites, flexible, Li–O_2 batteries

Received: February 10, 2018
Revised: May 15, 2018
Published online: July 25, 2018

[1] G. Girishkumar, B. McCloskey, A. C. Luntz, S. Swanson, W. Wilcke, *J. Phys. Chem. Lett.* **2010**, *1*, 2193.
[2] K. M. Abraham, Z. Jiang, *J. Electrochem. Soc.* **1996**, *143*, 1.
[3] L. Johnson, C. Li, Z. Liu, Y. Chen, S. A. Freunberger, P. C. Ashok, B. B. Praveen, K. Dholakia, J.-M. Tarascon, P. G. Bruce, *Nat. Chem.* **2014**, *6*, 1091.
[4] J. Zhu, Z. Xu, B. Lu, *Nano Energy* **2014**, *7*, 114.
[5] T. Danner, B. Horstmann, D. Wittmaier, N. Wagner, W. G. Bessler, *J. Power Sources* **2014**, *264*, 320.
[6] F. Li, H. Kitaura, H. Zhou, *Energy Environ. Sci.* **2013**, *6*, 2302.
[7] Q. Liu, Z. Chang, Z. Li, X. Zhang, *Small Methods* **2018**, *2*, 1700231.
[8] P. Tan, B. Chen, H. Xu, H. Zhang, W. Cai, M. Ni, M. Liu, Z. Shao, *Energy Environ. Sci.* **2017**, *10*, 2056.
[9] Q.-C. Zhu, S.-M. Xu, M. M. Harris, C. Ma, Y.-S. Liu, X. Wei, H.-S. Xu, Y.-X. Zhou, Y.-C. Cao, K.-X. Wang, J.-S. Chen, *Adv. Funct. Mater.* **2016**, *26*, 8514.

[10] Q. C. Zhu, F. H. Du, S. M. Xu, Z. K. Wang, K. X. Wang, J. S. Chen, *ACS Appl. Mater. Interfaces* **2016**, *8*, 3868.
[11] Y. Cui, Z. Wen, Y. Liu, *Energy Environ. Sci.* **2011**, *4*, 4727.
[12] M. M. Ottakam Thotiyl, S. A. Freunberger, Z. Peng, P. G. Bruce, *J. Am. Chem. Soc.* **2013**, *135*, 494.
[13] W.-B. Luo, X.-W. Gao, S.-L. Chou, J.-Z. Wang, H.-K. Liu, *Adv. Mater.* **2015**, *27*, 6862.
[14] W. B. Luo, X. W. Gao, D. Q. Shi, S. L. Chou, J. Z. Wang, H. K. Liu, *Small* **2016**, *12*, 3031.
[15] G. Yang, X. Xu, W. Yan, H. Yang, S. Ding, *Electrochim. Acta* **2014**, *137*, 462.
[16] G. Zhou, J. Zhu, Y. Chen, L. Mei, X. Duan, G. Zhang, L. Chen, T. Wang, B. Lu, *Electrochim. Acta* **2014**, *123*, 450.
[17] Y. B. Yin, J. J. Xu, Q. C. Liu, X. B. Zhang, *Adv. Mater.* **2016**, *28*, 7494.
[18] Z. Jian, P. Liu, F. Li, P. He, X. Guo, M. Chen, H. Zhou, *Angew. Chem., Int. Ed.* **2014**, *53*, 442.
[19] E. Yilmaz, C. Yogi, K. Yamanaka, T. Ohta, H. R. Byon, *Nano Lett.* **2013**, *13*, 4679.
[20] F. Li, D.-M. Tang, T. Zhang, K. Liao, P. He, D. Golberg, A. Yamada, H. Zhou, *Adv. Energy Mater.* **2015**, *5*, 1500294.
[21] J. Xie, X. Yao, I. P. Madden, D. E. Jiang, L. Y. Chou, C. K. Tsung, D. Wang, *J. Am. Chem. Soc.* **2014**, *136*, 8903.
[22] J. Cao, S. Liu, J. Xie, S. Zhang, G. Cao, X. Zhao, *ACS Catal.* **2015**, *5*, 241.
[23] P. Zhang, R. Wang, M. He, J. Lang, S. Xu, X. Yan, *Adv. Funct. Mater.* **2016**, *26*, 1354.
[24] M. Asadi, B. Kumar, C. Liu, P. Phillips, P. Yasaei, A. Behranginia, P. Zapol, R. F. Klie, L. A. Curtiss, A. Salehi-Khojin, *ACS Nano* **2016**, *10*, 2167.
[25] S. H. Oh, R. Black, E. Pomerantseva, J. H. Lee, L. F. Nazar, *Nat. Chem.* **2012**, *4*, 1004.
[26] J. Huang, B. Zhang, Y. Y. Xie, W. W. K. Lye, Z.-L. Xu, S. Abouali, M. Akbari Garakani, J.-Q. Huang, T.-Y. Zhang, B. Huang, J.-K. Kim, *Carbon* **2016**, *100*, 329.
[27] J.-L. Ma, F.-L. Meng, D. Xu, X.-B. Zhang, *Energy Storage Mater.* **2017**, *6*, 1.
[28] D. Ji, S. Peng, D. Safanama, H. Yu, L. Li, G. Yang, X. Qin, M. Srinivasan, S. Adams, S. Ramakrishna, *Chem. Mater.* **2017**, *29*, 1665.
[29] J. Jiang, L. Huang, X. Liu, L. Ai, *ACS Appl. Mater. Interfaces* **2017**, *9*, 7193.
[30] X. Li, Z. Niu, J. Jiang, L. Ai, *J. Mater. Chem. A* **2016**, *4*, 3204.
[31] B. Zhang, F. Kang, J.-M. Tarascon, J.-K. Kim, *Prog. Mater. Sci.* **2016**, *76*, 319.
[32] M. S. A. Rahaman, A. F. Ismail, A. Mustafa, *Polym. Degrad. Stability* **2007**, *92*, 1421.
[33] Y. Qiu, G. Li, Y. Hou, Z. Pan, H. Li, W. Li, M. Liu, F. Ye, X. Yang, Y. Zhang, *Chem. Mater.* **2015**, *27*, 1194.
[34] X.-Y. Yang, J.-J. Xu, Z.-W. Chang, D. Bao, Y.-B. Yin, T. Liu, J.-M. Yan, D.-P. Liu, Y. Zhang, X.-B. Zhang, *Adv. Energy Mater.* **2018**, *8*, 1702242.
[35] Y. Chen, X. Li, K. Park, J. Song, J. Hong, L. Zhou, Y. W. Mai, H. Huang, J. B. Goodenough, *J. Am. Chem. Soc.* **2013**, *135*, 16280.
[36] K.-H. Liu, H.-X. Zhong, X.-Y. Yang, D. Bao, F.-L. Meng, J.-M. Yan, X.-B. Zhang, *Green Chem.* **2017**, *19*, 4284.
[37] W. Ni, S. Liu, Y. Fei, Y. He, X. Ma, L. Lu, Y. Deng, *J. Mater. Chem. A* **2016**, *4*, 7746.
[38] R. R. Mitchell, B. M. Gallant, C. V. Thompson, Y. Shao-Horn, *Energy Environ. Sci.* **2011**, *4*, 2952.
[39] Z.-w. Chang, J.-j. Xu, Q.-c. Liu, L. Li, X.-b. Zhang, *Adv. Energy Mater.* **2015**, *5*, 1500633.
[40] T. Sun, L. Xu, S. Li, W. Chai, Y. Huang, Y. Yan, J. Chen, *Appl. Catal., B* **2016**, *193*, 1.
[41] F. Meng, H. Zhong, J. Yan, X. Zhang, *Nano Res.* **2017**, *10*, 4436.
[42] Y. Qi, H. Zhang, N. Du, D. Yang, *J. Mater. Chem. A* **2013**, *1*, 2337.
[43] Z.-H. Sheng, L. Shao, J.-J. Chen, W.-J. Bao, F.-B. Wang, X.-H. Xia, *ACS Nano* **2011**, *5*, 4350.
[44] Y. Cao, H. Lu, Q. Hong, J. Bai, J. Wang, X. Li, *J. Power Sources* **2017**, *368*, 78.
[45] M. Du, K. Rui, Y. Chang, Y. Zhang, Z. Ma, W. Sun, Q. Yan, J. Zhu, W. Huang, *Small* **2017**, *14*, 1702770.
[46] M. Huang, K. Mi, J. Zhang, H. Liu, T. Yu, A. Yuan, Q. Kong, S. Xiong, *J. Mater. Chem. A* **2017**, *5*, 266.
[47] J. Wu, H. W. Park, A. Yu, D. Higgins, Z. Chen, *J. Phys. Chem. C* **2012**, *116*, 9427.
[48] H. Huang, Q. Wang, Q. Wei, Y. Huang, *Int. J. Hydrogen Energy* **2015**, *40*, 6072.
[49] Y. Tu, H. Li, D. Deng, J. Xiao, X. Cui, D. Ding, M. Chen, X. Bao, *Nano Energy* **2016**, *30*, 877.
[50] R. R. Mitchell, B. M. Gallant, Y. Shao-Horn, C. V. Thompson, *J. Phys. Chem. Lett.* **2013**, *4*, 1060.
[51] Z.-L. Wang, D. Xu, J.-J. Xu, L.-L. Zhang, X.-B. Zhang, *Adv. Funct. Mater.* **2012**, *22*, 3699.
[52] R. Singhal, V. Kalra, *RSC Adv.* **2016**, *6*, 103072.
[53] J. Li, M. Zou, L. Chen, Z. Huang, L. Guan, *J. Mater. Chem. A* **2014**, *2*, 10634.
[54] X. Gao, Y. Chen, L. Johnson, P. G. Bruce, *Nat. Mater.* **2016**, *15*, 882.
[55] H. K. Lim, H. D. Lim, K. Y. Park, D. H. Seo, H. Gwon, J. Hong, W. A. Goddard 3rd, H. Kim, K. Kang, *J. Am. Chem. Soc.* **2013**, *135*, 9733.
[56] Z. H. Cui, X. X. Guo, H. Li, *Energy Environ. Sci.* **2015**, *8*, 182.
[57] J. J. Xu, Z. W. Chang, Y. B. Yin, X. B. Zhang, *ACS Cent. Sci.* **2017**, *3*, 598.
[58] J. J. Xu, Z. W. Chang, Y. Wang, D. P. Liu, Y. Zhang, X. B. Zhang, *Adv. Mater.* **2016**, *28*, 9620.
[59] R. Choi, J. Jung, G. Kim, K. Song, Y. I. Kim, S. C Jung, Y. K. Han, H. Song, Y. M. Kang, *Energy Environ. Sci.* **2014**, *7*, 1362.